

Postseismic Fault Healing on the Rupture Zone of the 1999 M 7.1 Hector Mine, California, Earthquake

by Yong-Gang Li, John E. Vidale, Steven M. Day, David D. Oglesby, and Elizabeth Cochran

Abstract We probed the rupture zone of the October 1999 M 7.1 Hector Mine earthquake using repeated near-surface explosions in October 2000 and November 2001. Three dense linear seismic arrays were deployed across the north and south Lavic Lake faults (LLFs) that broke to the surface in the mainshock and across the Bullion fault (BF) that experienced minor slip in that event. Two explosions each year were detonated in the rupture zone, one on the middle and one on the south LLF. We found that P and S velocities of fault-zone rocks increased by $\sim 0.7\%$ – 1.4% and $\sim 0.5\%$ – 1.0% between 2000 and 2001, respectively. In contrast, the velocities for P and S waves in surrounding rocks increased much less. This trend indicates that the Hector Mine rupture zone has been healing by strengthening after the mainshock, most likely due to the closure of cracks that opened during the 1999 earthquake. The observed fault-zone strength recovery is consistent with an apparent crack density decrease of 1.5% within the rupture zone. The ratio of travel-time decrease for P to S waves was 0.72, consistent with partially fluid-filled cracks near the fault zone. This restrengthening is similar to that observed after the 1992 M 7.4 Landers earthquake, which occurred 25 km to the west (Li and Vidale, 2001). We also find that the velocity increase with time varies from one fault segment to another at the Hector Mine rupture zone. We see greater changes on the LLFs than on the BF, and the greatest change is on the middle LLF at shallow depth. We tentatively conclude that greater damage was inflicted, and thus greater healing is observed, in regions with larger slip in the mainshock.

Introduction

The fault zone undergoes high, fluctuating stress and pervasive cracking during an earthquake. Extensive research in the field, in laboratories, and with numerical simulations has addressed this phenomenon (e.g., Dieterich, 1978; Aki, 1984; Mooney and Ginzburg, 1986; Scholz, 1990; Rice, 1992; Kanamori, 1994). There is evidence that the strength of the fault zone varies over the earthquake cycle (Vidale *et al.*, 1994; Marone *et al.*, 1995; Li *et al.*, 1998b), consistent with state- and rate-dependent healing models (Dieterich, 1972). Rupture models that involve variations in fault-zone fluid pressure over the earthquake cycle have been proposed (Sibson, 1977; Blanpied *et al.*, 1992, 1998; Olsen *et al.*, 1998). Structural fault variations (e.g., Das and Aki, 1977; Rice, 1980) and rheological fault variations (e.g., Angevine *et al.*, 1982; Walder and Nur, 1984; Peltzer *et al.*, 1998) as well as variations in strength and stress (e.g., Wesson and Ellsworth, 1973; Vidale *et al.*, 1994; Beroza *et al.*, 1995) may affect the earthquake rupture. Thus, knowledge of spatial and temporal variations in fault physical properties will help predict the behavior of future earthquakes.

We have the particularly favorable situation in the

Landers and Hector Mine earthquakes of probing the evolution of active faults that had recently undergone large displacements. These events broke the ground surface, allowing us to record the fault-zone trapped waves generated by aftershocks and near-surface explosions. With these waves, we have studied the internal structure and continuity of the active fault planes at Landers (Li *et al.*, 1994a,b, 1999, 2000) and Hector Mine (Li *et al.*, 2002a,b). At Landers, observations and modeling of trapped waves revealed a ~ 200 -m-wide wave guide on the Johnson Valley fault to the seismogenic depth. Within the wave guide, seismic velocities are reduced by 40%–50% from wall-rock velocities and Q is 20–50. We interpreted that the trapped waves mark a thoroughly cracked low-velocity, low- Q zone along the Landers faults, as suggested by fracture mechanics (e.g., Rice, 1980; Papageorgiou and Aki, 1983; Cowie and Scholz, 1992). This zone is partly the transient result of the dynamic rupture in the 1992 M 7.4 earthquake and probably also represents the accumulated damage from many previous earthquakes. Our repeated seismic surveys using explosions at the Johnson Valley fault in 1994, 1996, and 1998 showed that the shear

velocity within the rupture zone increased by $\sim 1.2\%$ between 1994 and 1996 and by an additional $\sim 0.7\%$ between 1996 and 1998 (Li and Vidale, 2001). This trend indicates that the Landers rupture zone has been healing after the mainshock, most likely due to the closure of cracks that opened during the 1992 earthquake. The ratio of decrease in travel time for P to S waves evolved from 0.75 in the earlier 2 years to 0.65 in the later 2 years, suggesting that cracks near the fault zone are partially fluid filled and have become more fluid saturated with time. Summing up, the Landers fault at shallow depth has displayed healing after the mainshock, supporting the existence of a broken-then-healing earthquake cycle in the evolution of active faults.

The M 7.1 Hector Mine earthquake occurred on 16 October 1999, ~ 25 km east of Landers. This quake produced a 40-km-long surface rupture, breaking both the Lavic Lake fault (LLF) and the southeast Bullion fault (BF) (Fig. 1). On the middle of the LLF in the Bullion Mountains, the faulting has a maximum right-lateral slip of 5 m and is relatively simple, with most of the surface slip on a single trace or closely spaced parallel traces. In contrast, the southern and northern portions of the rupture zone had a more complex faulting pattern with less slip (Scientists from USGS, SCEC,

and CDMG, 2000). Numerical modeling of observed micro-earthquake-generated fault-zone trapped waves have delineated a low-velocity and low- Q wave guide along the rupture zone on the LLF that is 75–100 m wide, with shear velocities reduced by $\sim 40\%$ – 50% from wall-rock velocities and a Q of 10–50 (Li *et al.*, 2002).

In this article, we report the results from our repeated near-surface explosions at the Hector Mine rupture zone in October 2000 and November 2001. Repeated surveys revealed that the LLF, which was softened by the dynamic rupture in the M 7.1 Hector Mine earthquake of 1999, has regained strength with time.

Repeated Explosions in the Rupture Zone

In order to study shallow fault-zone structure (Li *et al.*, 2003) and search for temporal healing of the Hector Mine rupture zone, we detonated explosions within the rupture zone in October 2000 and repeated the explosions in November 2001. P , S , and fault-zone trapped waves from the explosions were recorded at three dense linear seismic arrays deployed across the rupture zone in the Bullion Mountains and Quackenbush. Figure 1 shows locations of seismic ar-

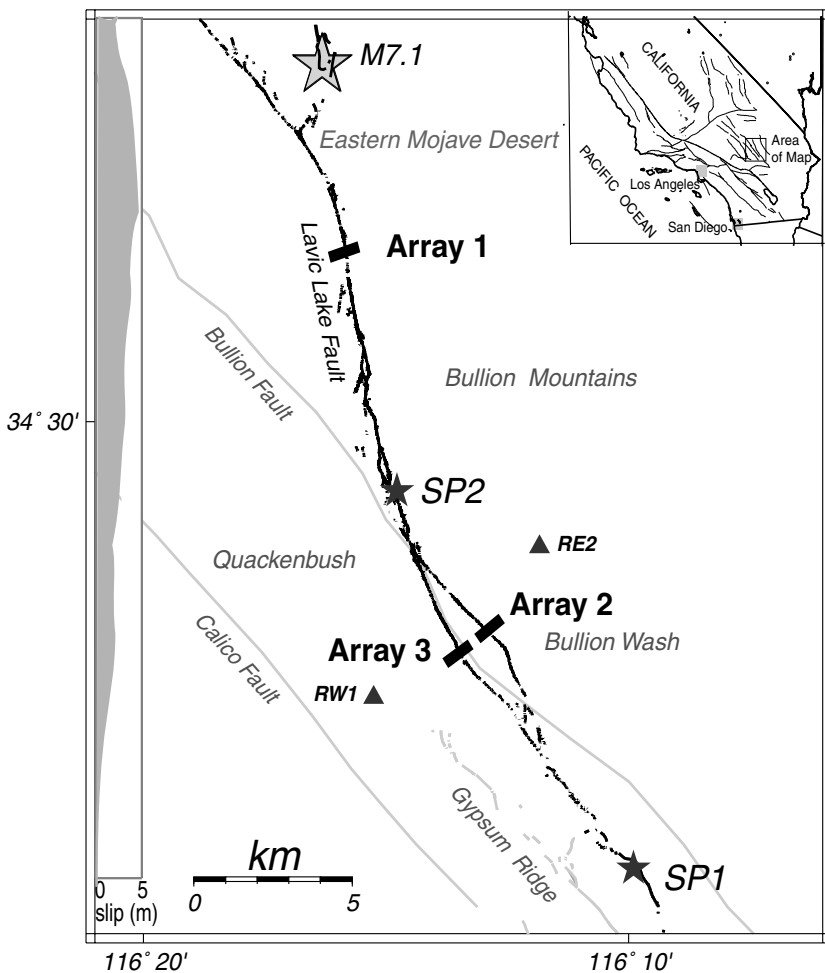


Figure 1. The locations of linear seismic arrays (heavy lines labeled array 1, 2, and 3) deployed across the LLF and BF and explosions (stars labeled SP1 and SP2) detonated in October 2000 and November 2001. RW1 and RE2 were remote stations deployed away from the rupture zone. Black irregular lines show mapped surface breaks of the October 1999 M 7.1 earthquake, and the right-lateral slip profile on the LLF is shown to the left of the rupture zone (Scientists from USGS, SCEC, and CDMG, 2000). The inset shows the location of the area of map. Gray lines show unbroken faults.

rays and shot points. The LLF experienced 4 m right-lateral slip at the site of array 1, which was ~ 6 km south of the 1999 *M* 7.1 Hector Mine earthquake epicenter. The rupture zone at the surface is ~ 75 m wide, including one major and several minor parallel faults with the mainshock slip. The lateral slips were ~ 1 m at the site of array 3 across the south LLF and 0.5 m at the site of array 2 across the southeast BF. The vertical slips were 0.3–0.5 m with the west side up at site array 2 but with the east side up at site array 3. The rupture extended 10 km further along the south LLF to Gypsum Ridge, while slip diminished quickly to the south on the southeast BF (Fig. 1). Fault slip at depth is probably more complicated than the slip at the surface (Ji *et al.*, 2002; Li *et al.*, 2002, 2003). The recurrence interval of faulting on the LLF and BF is thousands of years (Scientists from USGS, SCEC, and CDMG, 2000).

Array 1 was composed of 16 three-component stations along a 350-m-long line across the north LLF in the Bullion Mountains. Array 2 and array 3 were each 500 m long and composed of 18 stations. These two arrays were located 18 km south of the mainshock epicenter and ~ 1 km apart from each other. Station spacing in the arrays was not even, with 12.5-m separation for stations close to the main fault trace and 25- or 50-m spacing for farther stations. Station ST0, at the center of each array, was deployed on the main fault trace. The coordinates of station ST0 were $34^{\circ}\text{N}31.05'$ and $116^{\circ}\text{W}15.71'$ in array 1, $34^{\circ}\text{N}26.31'$ and $116^{\circ}\text{W}12.56'$ in array 2, and $34^{\circ}\text{N}25.91'$ and $116^{\circ}\text{W}13.21'$ in array 3. We also deployed two remote stations 3 km away from the rupture zone with coordinates of $34^{\circ}\text{N}24.11'$ and $116^{\circ}\text{W}15.82'$ at site RW1 and $34^{\circ}\text{N}28.22'$ and $116^{\circ}\text{W}11.82'$ at site RE2 (Fig. 1).

Each year, we used three-channel REFTEK recorders and three-component sensors (Mark Products 2-Hz L22) from the PASSCAL Instrument Center of Incorporated Research Institutions for Seismology. The three components of the sensor at each station were aligned vertical, parallel, and perpendicular to the fault trace. Sensors were reburied in the same holes to minimize wind noise and improve coupling. The signals were sampled at a rate of 1000/sec.

Two explosions were detonated in 40-m-deep shot holes drilled in the rupture zone at sites SP1 and SP2, located ~ 12.5 and ~ 25 km south of the mainshock epicenter, respectively. SP2 was close to the southern edge of the Bullion Mountains, where the LLF had experienced ~ 2.5 m of coseismic slip at surface in the mainshock. SP1 was close to the south end of the rupture zone near Gypsum Ridge, where the surface slip was less than 0.5 m. The shot holes required casing because of a soft weathering layer at the drilling sites. Each shot hole was loaded with 500 kg of chemical emulsions. The shot hole coordinates were $34^{\circ}\text{N}22.49'$ and $116^{\circ}\text{W}09.73'$ at SP1 and $34^{\circ}\text{N}27.74'$ and $116^{\circ}\text{W}14.77'$ at SP2. A REFTEK recorder was installed at the wellhead of each shot hole. The clocks of all recorders and shot times were synchronized through Global Positioning System. The

clock errors for recorders and the explosion controller were less than 0.001 sec.

We have previously used explosion-excited trapped waves to document the shallow rupture zone structure at Hector Mine to a depth of a few kilometers (Li *et al.*, 2003). In the following section, we show that data recorded for the same shot-array pairs in the repeated experiments reveal temporal changes in physical properties near the rupture of the 1999 *M* 7.1 Hector Mine earthquake.

Data Analysis

The recordings in repeated experiments in 2000 and 2001 reveal resolvable velocity increases. For example, Figure 2 shows three-component seismograms recorded at array 3 across the south LLF for the north shot SP2 detonated in 2000 and 2001. The repeated experiments produced nearly identical waveforms of *P*, *S*, and fault-zone trapped waves. *P* and *S* waves arrive ~ 1.7 and ~ 3.5 sec after the shot time. Trapped waves with relatively large amplitudes following *S* waves appeared at stations between ST0 and W8. Trapped waves are dominant from 5 until 12 sec, while showing multiple trapped wave trains. In Figure 3a, we overlaid the seismograms, aligning the shot times in the surveys from 2000 and 2001. The first arrivals of *P* waves registered at the wellhead geophone showed almost identical travel times in the repeated experiments. However, the travel times of the *P*, *S*, and trapped waves to stations of array 3, located ~ 4.5 km south of SP2, decreased several tens of milliseconds from 2000 to 2001. We measured the advances in travel time accurately in four time windows including the *P*, *S*, and trapped waves. Windows 1 and 2 include *P* and *S* waves, respectively. Windows 3 and 4 include fault-zone trapped waves. We cross-correlated each pair of recordings in four time windows for the same shot and same seismometer to obtain time differences between the 2000 and 2001 data. Examples with recordings at station ST0 of array 3 and the remote station RW1 are shown in Figure 3b. Note that travel-time advances in the vertical component are sometimes different from those in the perpendicular-to-fault component. We present the average value of measurements from the three components. The measured advances in arrival time were 23, 35, 55, and 90 msec for *P*, *S*, and trapped waves between 2000 and 2001. The absolute advances in arrival time increased progressively with the longer travel times for *P*, *S*, and trapped waves. These changes are much larger than the uncertainty in the origin time of the explosion. We measured the time shift of the first arrivals of *P* waves at the wellhead geophones for repeated explosions less than 2 msec and have taken account for this error in the measurements for array stations.

If the velocity changes were uniform in the crust that was sampled by these waves, the decrease in travel times would be straightforward to interpret. From $L = v_1 t_1 = v_2 t_2$, where L is the distance between the shot and array and $v_1 t_1$ and $v_2 t_2$ are the velocities and travel times in repeated ex-

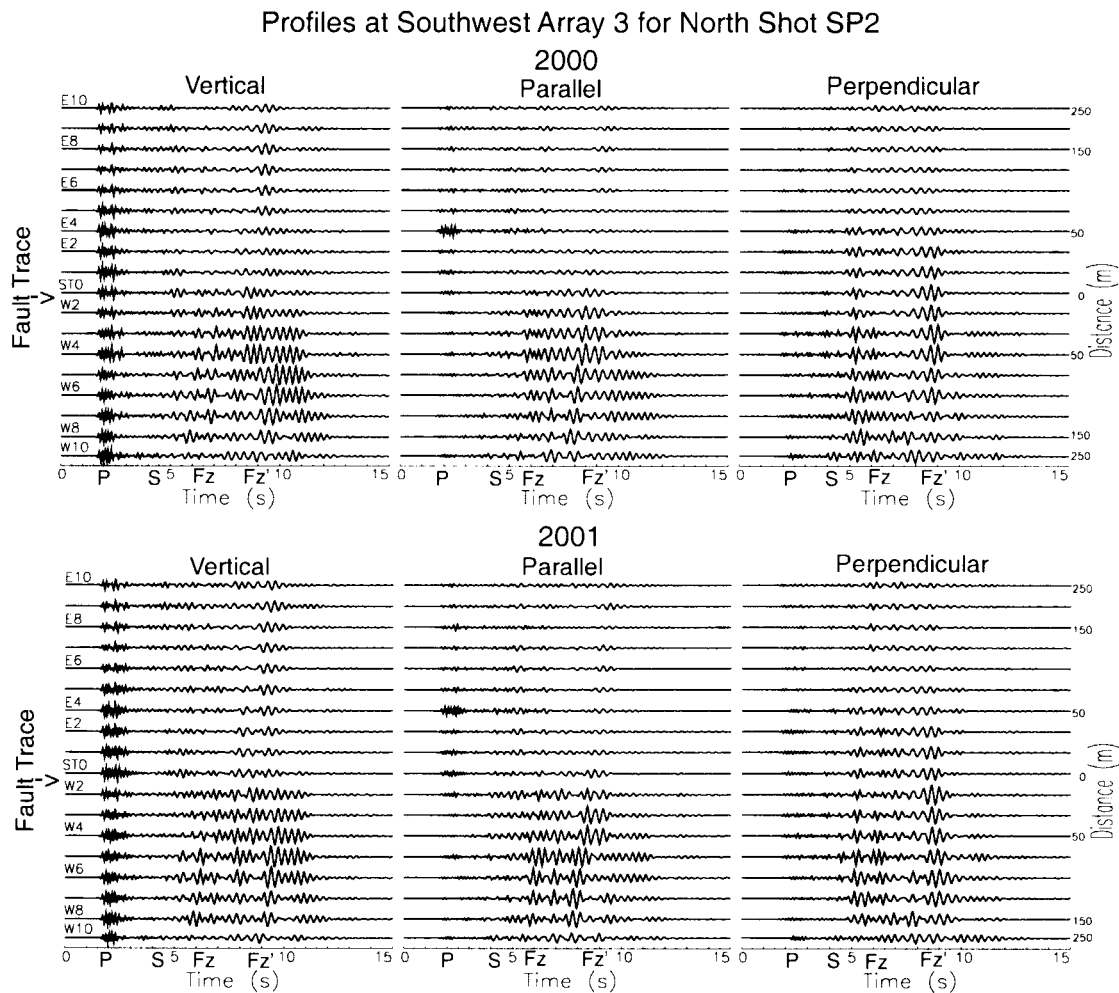


Figure 2. Three-component seismograms recorded at southwest array 3 across the south LLF for the north shot SP2 detonated in 2000 and 2001. Seismograms have been bandpass (3–15 Hz) filtered and are plotted using a common scale for all traces. The array was 500 m long with uneven station spacings, plotted at right of seismograms. Station ST0 was located on the main fault trace of the LLF. Station names beginning with “E” or “W” denote the station located east or west of the fault trace, although only the stations with even numbers are labeled. *P* and *S* waves arrive at ~1.7 and ~3.5 sec. Fault-zone trapped waves with large amplitudes and long duration appear between 5 and 12 sec at stations between ST0 and W7. “Fz” and “Fz'” denote the early and late wave trains of trapped waves. Similar waveforms were recorded in the repeated experiments.

periments, $v_2/v_1 = t_1/t_2$. For example, the *P* wave arrived 23 msec earlier in 2001, with a travel time of ~1.7 sec, so the *P*-wave velocity increased by ~1.4% between 2000 and 2001. Similarly, the *S* wave arrived 35 msec earlier in 2001, with travel time of ~3.5 sec, so the *S*-wave velocity increased by ~1.0%. Trapped waves in windows 3 and 4 with longer travel times had larger time advances than *P* and *S* waves, again resulting in an ~1.0% increase in velocity within the rupture zone (Table 1).

In contrast, the advances in travel times for *P* and *S* waves at remote stations RW1 and RE2 located ~3 km southwest and northeast of the rupture zone were much smaller than those at station W1 within the rupture zone for

the same shot. For example, cross-correlations of seismograms recorded at station RW1 show travel-time decreases of 6 and 9 msec for *P* and *S* waves between 2000 and 2001 (Fig. 3b). The *P* and *S* velocities increased by ~0.35% and ~0.26%, respectively, for surrounding rocks. We also note that trapped waves were not clear at station RW1 because it was located far away from the rupture zone.

Figure 4 shows three-component seismograms recorded at array 3 for shot SP1 detonated at the south end of the Hector Mine rupture zone, ~8 km from the array in 2001. *P* and *S* waves arrive at ~3 and ~6 sec, respectively. Fault-zone trapped waves appear at stations located in the rupture zone and are prominent between 13 and 17 sec. The sepa-

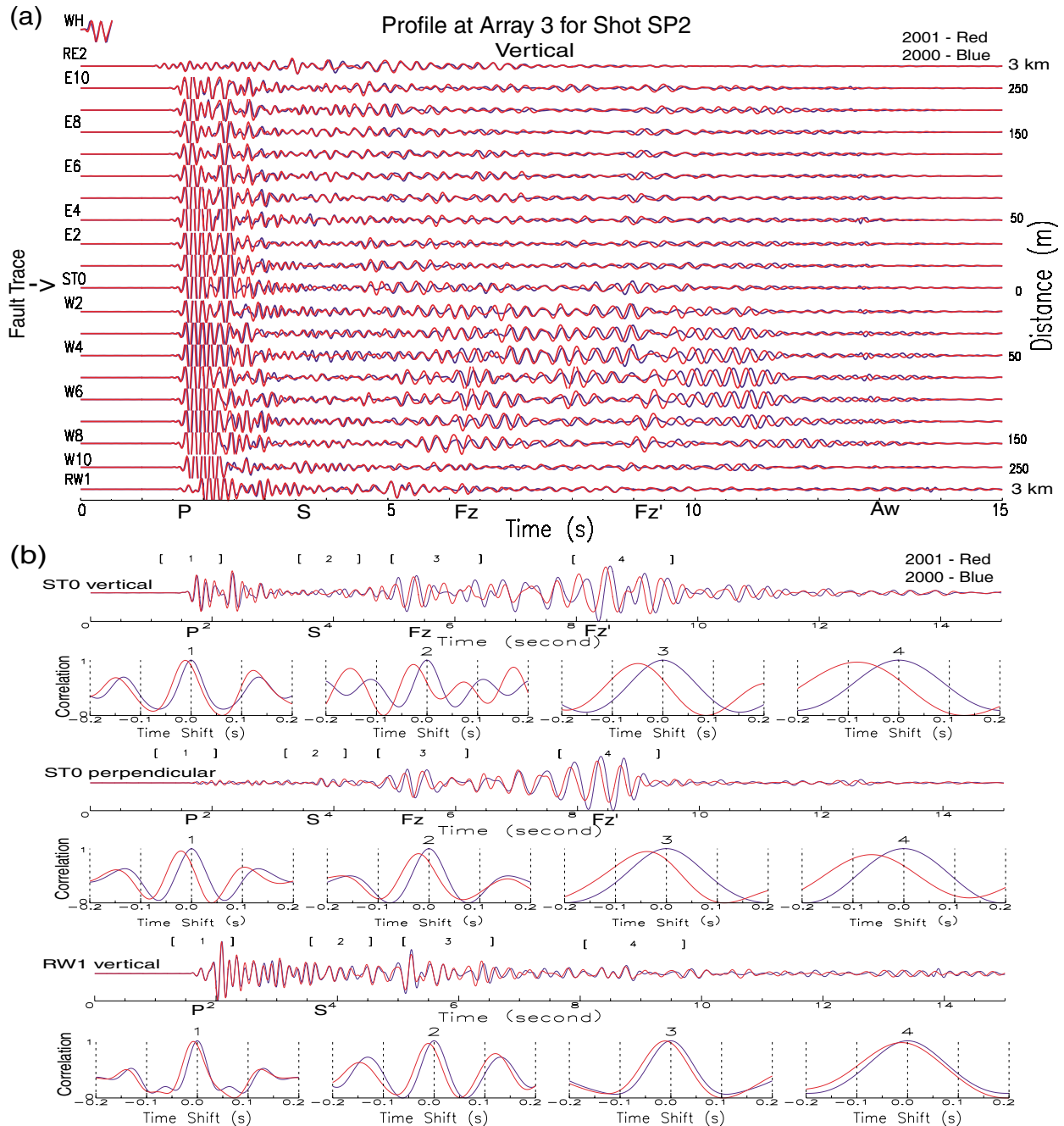


Figure 3. (a) Vertical-component seismograms recorded at array 3 for shot SP2 in 2000 and 2001. Seismograms have been bandpass (2–8 Hz) filtered and are plotted using a common scale for all traces. Other notations are the same as in Figure 2. Airwaves (Aw) arrive at 13 sec. Similar waveforms were recorded in repeated experiments, but waves traveled faster in 2001 than in 2000. WH denotes the station located at the wellhead of the shot hole; only the first arrivals of *P* waves are plotted here because the late part of the seismograms were clipped. “RW1” and “RE2” denote two remote stations located ~3 km southwest and northeast of array 3. (b) Vertical- and perpendicular-to-fault component seismograms recorded at station ST0 of array 3 and the remote station RW1 for shot SP2 in 2000 and 2001. Seismograms have been bandpass (3–10 Hz) filtered. Station ST0 was located at the LLF trace. Autocorrelations (blue lines) of seismograms in 2000 and cross-correlations (red lines) of recordings at the same station in 2000 and 2001 are shown for four time windows (1–4) including *P*, *S*, and early and late trapped waves, respectively. The length of the first two windows is 0.5 sec; the length of the latter two windows is 1 sec. The peak of autocorrelation curve is at zero lag time in each window. The negative time shift indicates time advance. The time advances of the waves were greater at station ST0 than at the remote station RW1.

Table 1
Travel-Time and Velocity Changes of *P*, *S*, and Trapped Waves in Figures 3, 5, 6, and 7

	t_p (sec)	t_s (sec)	t_{fz1} (sec)	t_{fz2} (sec)	Δt_p (ms)	Δt_s (ms)	Δt_{fz1} (ms)	Δt_{fz2} (ms)	Δv_p (%)	Δv_s (%)	Δv_{fz1} (%)	Δv_{fz2} (%)
Array 1, SP1	4.8	7.5	10.0	12.0	28	36	50	60	0.59	0.48	0.50	0.50
Array 1, SP2	2.0	3.7	5.0	7.0	18	25	35	47	0.91	0.68	0.70	0.67
Array 2, SP1	3.0	6.0	8.5	13.5	15	22	30	45	0.50	0.35	0.35	0.33
Array 2, SP2	1.7	3.5	5.5	8.5	15	21	33	50	0.88	0.60	0.61	0.59
Array 3, SP1	3.0	6.0	8.5	13.5	25	36	48	80	0.84	0.60	0.57	0.60
Array 3, SP2	1.7	3.5	5.5	8.5	23	35	55	90	1.40	1.00	1.00	1.10

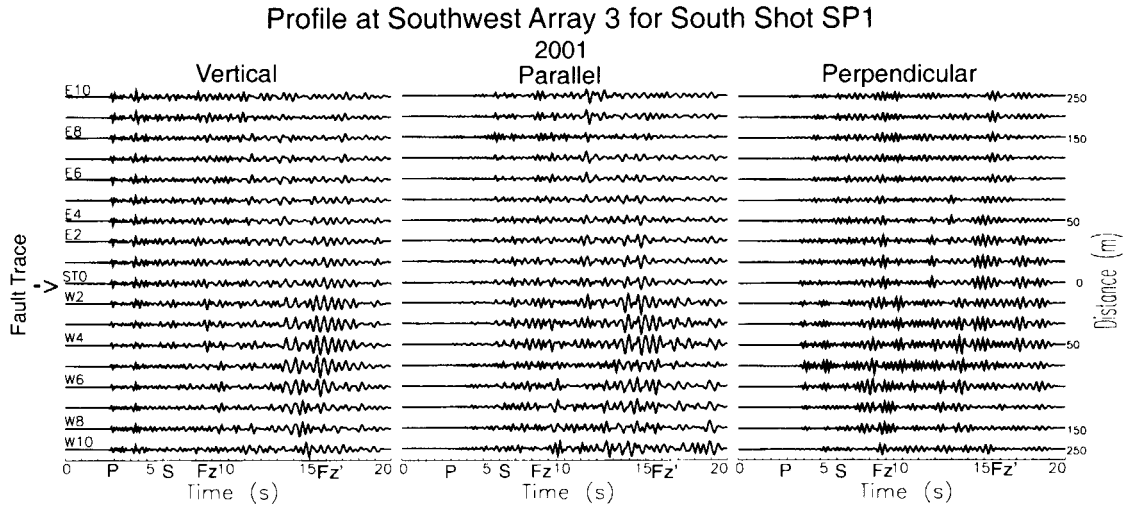


Figure 4. Three-component seismograms recorded at southwest array 3 across the south LLF for the south shot SP1 detonated in 2001. Seismograms have been bandpass (3–15 Hz) filtered and are plotted using a common scale for all traces. *P* and *S* waves arrive at ~ 3 and ~ 6 sec. Fault-zone trapped waves appear between 9 and 17 sec at stations between ST0 and W7. “Fz” and “Fz’” denote the early and late wave trains of trapped waves.

ration between *S* and trapped waves from the farther shot SP1 are larger than that from SP2 to array 3. In Figure 5, we show overlapping vertical-component seismograms and waveform cross-correlations between the 2000 and 2001 recordings. Again, we observed similar waveforms in repeated surveys, but the waves traveled faster in 2001 than in 2000. For example, the measured advances in travel time at station W5 located within the rupture zone were 25, 36, 48, and 80 msec in time windows 1–4. Accordingly, the velocity of the *P* wave with a travel time of 3 sec increased by 0.84%. The velocity of *S* wave, with a travel time of 6 sec, increased by 0.6% between 2000 and 2001. Trapped waves in windows 3 and 4 with longer travel times had larger time advances than *P* and *S* waves, resulting in $\sim 0.6\%$ increases in velocity within the rupture zone. However, the time advances measured at station E8, located 200 m east of the LLF, are smaller than those measured at station W5 located within the rupture zone. We note that the velocity increases on the middle LLF between SP2 and array 3 are greater than those on the south LLF (which had also smaller coseismic displacement) between SP1 and array 3. In contrast, the remote stations RW1

and RE2 registered much smaller travel-time advances for the same shot between 2000 and 2001. The velocities for *P* and *S* waves in surrounding rocks increased by $\sim 0.3\%$ and $\sim 0.23\%$, respectively. Trapped waves were not clear at remote stations because they were located far away from the rupture zone.

The data recorded at the north seismic array 1 revealed a velocity increase with time on the north LLF. Figure 6a illustrates the overlaying of vertical-component seismograms at array 1 for the north shot SP2 detonated 7.5 km from the array in 200 and 2001. *P*, *S*, and trapped waves arrived at ~ 2 and ~ 3.7 sec, respectively. Trapped waves appeared between 5 and 8 sec and were prominent at stations between E3 and W4 close to the main fault trace. Based on the distance between stations E3 and W4 in which prominent trapped waves were exhibited, we estimate that the width of the rupture zone (low-velocity wave guide) on the north LLF at this site is 75–100 m. All phases of seismic waves traveled faster in 2001 than in 2000. In Figure 6a, we also show waveform cross-correlations between 2000 and 2001 at station ST0 located within the rupture zone. We measured ad-

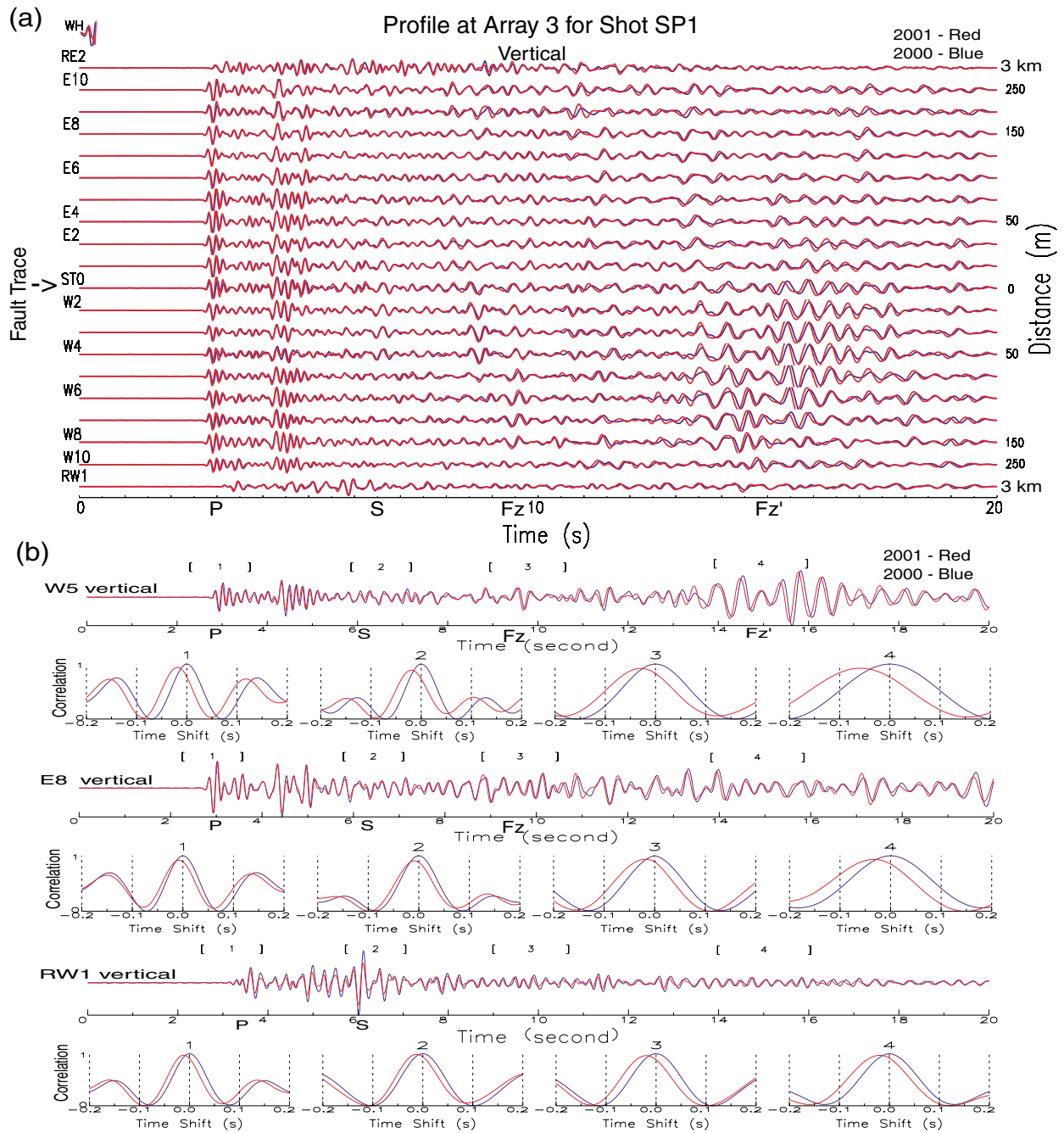


Figure 5. (a) Vertical-component seismograms (2–8 Hz) at array 3 for shot SP1 in 2000 and 2001. Other notations are the same as in Figure 4. (b) Vertical-component seismograms recorded at stations W5, E8 of array 3 and the remote station RW1 for shot SP1 in 2000 and 2001. Seismograms have been bandpass (3–10 Hz) filtered. Autocorrelations (blue lines) of seismograms in 2000 and cross-correlations (red lines) of recordings at the same station in 2000 and 2001 are shown for four time windows (1–4) including *P*, *S*, and early and late trapped waves, respectively. Greater time advances of waves in 2001 than in 2000 were registered at station W5, located within the rupture zone, than at station E8, located away from the rupture zone. Small time advances were registered at the remote station RW1.

vances in travel time of 18, 25, 35, and 47 msec in time windows 1–4 including *P*, *S*, and trapped waves. The velocity of the *P* wave with a travel time of ~ 2 sec increased by $\sim 0.9\%$, while the velocity of the *S* wave with a travel time of ~ 3.7 sec increased by $\sim 0.68\%$ within the rupture zone between 2000 and 2001. Trapped waves in windows 3 and 4 showed a 0.65% – 0.7% increase in velocity.

Figure 6b illustrates seismograms recorded at north array 1 for south shot SP1 in 2000 and 2001. Again, we obtained similar waveforms in repeated surveys, but the waves traveled faster in 2001 than in 2000. The distance between the shot and array was ~ 20 km. *P*, *S*, and trapped waves appear at about 4.8, 7.5, and 9–13 sec. Travel times of *P*, *S*, and trapped waves from SP1 to array 1 and array 3 were larger than those from SP2 to array 1, although they were not proportional to the distance between the shot and arrays because waves from SP1 to array 1 traveled in the deeper crust with higher velocities. We note that the time duration of the dominant trapped waves after *S* waves increased with travel distances between the shots and array, showing that the trapped waves were not caused by the local structure near the array site but produced by the low-velocity wave guide along the rupture surface at depth. Figure 6b also shows waveform cross-correlations of seismograms recorded at station W1 between 2000 and 2001 in four time windows, revealing that *P*, *S*, and trapped waves advanced by 28, 36, 50, and 60 msec, respectively. Accordingly, the *P*-wave velocity increased by $\sim 0.59\%$, and the velocities of *S* and trapped waves increased by $\sim 0.48\%$ within the rupture zone at deep level.

We then examined the data recorded at array 2 across the southeast BF. Station ST0 of array 2 was deployed on the surface breaks at this site. The west part of the array was on a hill of sedimentary rock, and the east part of the array was in soft sand (Bullion wash in Fig. 1). The ground motion at array 2 was qualitatively different from that at the other two arrays, but still agrees in general with the observations made previously. Figure 7a shows similar waveforms of seismograms recorded at array 2 for the north shot SP2 in 2000 and 2001. Fault-zone guided waves from SP2 traveled along the middle LLF and then along the southeast BF. These waves might be affected adversely by the complicated geological conditions at this site (Li *et al.*, 2003). We have discussed the effect of near-surface structures on fault-zone trapped waves in our previous numerical investigation of low-velocity wave-guide trapping efficiency (Li and Vidale, 1996). Figure 7a also shows waveform cross-correlations between 2000 and 2001 recordings in the four time windows at station E2 of array 2. The results show that *P*, *S*, and trapped waves traveled faster in 2001 than in 2000, but with smaller time advances than those at array 3 across the LLF (Fig. 3; Table 1), although the distances from SP2 to array 2 and array 3 were almost the same. This difference may be related to the smaller coseismic slip that occurred on the southeast BF (in the area of array 2) in the 1999 earthquake compared with slip on the LLF (in the area of array 3). In

fact, we observed very small travel-time advances at array 2 for the south shot SP1 detonated at the southernmost LLF (Fig. 7b). The time advances for *P* and *S* waves are 0.5% and 0.35% between 2000 and 2001. However, this lack of apparent velocity increase could also be due to decreased healing in the country rock between SP1 on the LLF and array 2 across the BF, in comparison to the fault-zone path between other source-receiver pairs.

In summary, Figure 8 shows the percentage decrease in travel time of *P*, *S*, and trapped waves at all stations on arrays 1, 2, and 3 for shots SP1 and SP2 between 2000 and 2001. Larger changes in arrival times were observed at stations located close to the fault trace, with a velocity increase of $\sim 0.7\%$ – 1.4% for *P* waves and $\sim 0.5\%$ – 1.0% for *S* waves between 2000 and 2001. In contrast, the velocities to stations located far away from the rupture zone increased by $\sim 0.45\%$ for *P* waves and $\sim 0.35\%$ for *S* waves between 2000 and 2001. Based on the width of the zone exhibiting larger arrival-time decreases between 2000 and 2001, we estimate that the Hector Mine rupture zone width in the top few kilometers is about 100 m. Note that there was little difference between the healing rate for close and far stations in array 2 from shot SP1.

Figure 8 also shows the ratio of decrease in travel time for *P* to *S* waves ($\Delta t_p/\Delta t_s$) for all repeated shot-receiver pairs. The mean $\Delta t_p/\Delta t_s$ was 0.71 with a standard deviation of 0.04 for paths from the north shot SP2, while the mean $\Delta t_p/\Delta t_s$ was 0.74 with a standard deviation of 0.03 for paths from the south shot SP1 between 2000 and 2001. The mean $\Delta t_p/\Delta t_s$ for all measurements was 0.725 with a standard deviation of 0.035 between 2000 and 2001. We note that this ratio is relatively small at stations within the rupture zone for shot SP2. The calculated $\Delta t_p/\Delta t_s$ for remote stations RW1 and RE2 located at 3 km away from the rupture zone was 0.79 ± 0.22 .

Conclusions and Discussion

Our observations in the repeated seismic surveys at the Hector Mine rupture zone indicate that the rupture zone has been strengthening (healing), by a rigidity increasing with time. This effect is most likely due to the closure of cracks that opened during the 1999 M 7.1 mainshock. We found that the velocity increase varied from one rupture segment to another. The increases in velocity observed on the north LLF, in the hard-rock mountains, were smaller than those on the middle LLF in softer sedimentary basement, but larger than those on the southernmost LLF. This difference in healing rate between different rupture segments could be due to either differences in rock type or differences in the amount of slip and damage. The healing rate may be depth dependent, too. Because we only captured healing between 1 and 2 years after the Hector Mine earthquake, we may have missed the information in the earliest stage of fault healing.

In our previous work, we have delineated the Hector Mine rupture zone in 3D (Li *et al.*, 2002, 2003). The zone

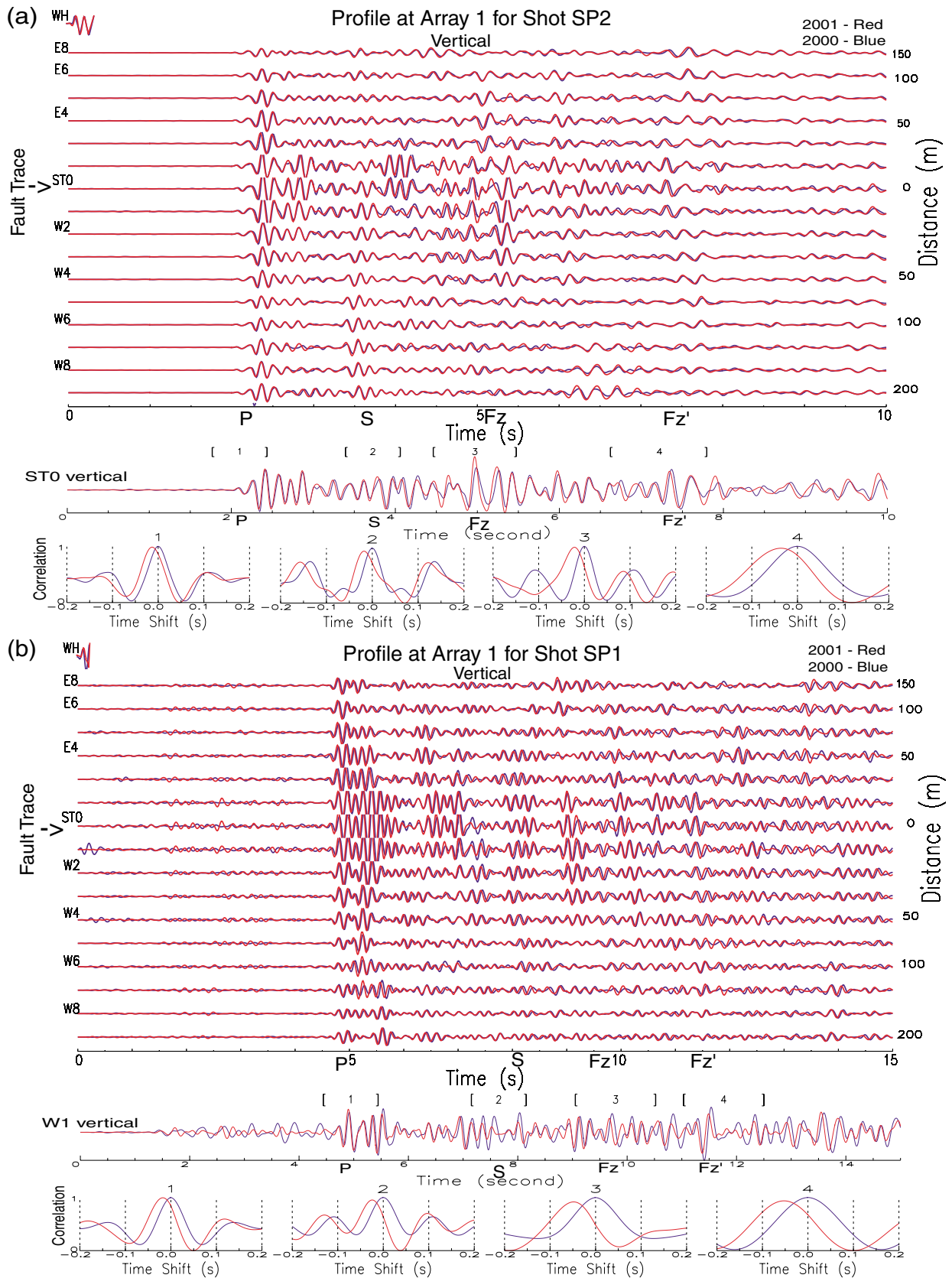


Figure 6. (a) Vertical component seismograms recorded at array 1 across the north LLF for the north shot SP2 detonated in 2000 and 2001. Seismograms have been bandpass (2–8 Hz) filtered and are plotted using a common scale for all traces. *P* and *S* waves arrive at ~ 2 and ~ 4 sec. Trapped waves appear between 5 and 8 sec at stations between E3 and W4. Autocorrelations (blue lines) of seismograms in 2000 and cross-correlations (red lines) of recordings at station ST0 in 2000 and 2001 are shown for four time windows (1–4). Seismograms have been bandpass (3–10 Hz) filtered. Other notations are the same as in Figure 3. (b) Vertical-component seismograms (2–6 Hz) recorded at array 1 for the south shot SP1 detonated in 2000 and 2001. *P* and *S* waves arrive at ~ 5 and ~ 8 sec. Trapped waves appear between 9 and 13 sec at stations between E3 and W4. Similar waveforms were recorded in repeated experiments, but waves traveled faster in 2001 than in 2000. Autocorrelations (blue lines) of seismograms in 2000 and cross-correlations (red lines) of recordings at station W1 in 2000 and 2001 are shown for four time windows (1–4). Seismograms have been bandpass (3–10 Hz) filtered. Other notations are the same as in Figure 5.

is about 75–100 m wide and has a velocity reduction of 40%–50% from wall-rock velocities and a Q of 10–60. Within the zone, *S* velocities are ~ 1.0 to ~ 2.6 km/sec in the depth range between the surface and ~ 10 km. The rupture zone structure is not uniform with depth because the increasing pressure with increasing depth will strongly reduce the crack density and probably increase the rate of healing of damage caused by earthquakes (Sibson, 1977, 1982; Byerlee, 1990; Rice, 1992). It is also likely to influence the development of fault gouge (Scholz, 1990; Marone, 1998) and the mineralogy of the rocks (Angevine and Turcotte, 1983). Thus, the fault-zone properties may depend on depth.

We interpret that the distinct low-velocity wave guide inferred by trapped waves in large part represents the process zone of inelastic deformation around the propagating crack tip in the 1999 Hector Mine earthquake, as predicted by existing fault-zone rupture models (e.g., Rice, 1980; Papageorgiou and Aki, 1983; Cowie and Scholz, 1992). Although the low-velocity wave guide along the rupture surface probably also represents a damage zone that has accumulated over geological time, it is likely that the wave guide has been significantly weakened by the dynamic rupture in the most recent major earthquake. However, note that the location of the surface slip at the edge of the trapped-wave-derived fault zone rather than symmetrically at its center (Fig. 2) may imply that the fault zone has a significant cumulative damage component and may represent the locus of planes that have slipped in previous events. When the fault slips on a plane in the fault zone, it may preferentially damage the already weakened rocks in the fault zone, even though those rocks are not symmetrically distributed on either side of the fault (Chester *et al.*, 1993). Conversely, the location of the fault plane in the weak zone may greatly affect the propagation of rupture and slip (e.g., Harris and Day, 1997). Dynamic

rupture models of this event may help to further examine these effects.

Both the Hector Mine and Landers earthquakes occurred in the eastern Mojave shear zone and are characterized by high stress drop (150–200 bar) and long earthquake cycle (several thousands of years) (Sieh *et al.*, 1993; Sauber *et al.*, 1994). The observed reduction of velocities on the LLF caused by dynamic rupture in the 1999 M 7.1 Hector Mine earthquake is approximately the same as that on the Landers fault zone, indicating that the fault-zone rock was damaged to a similar degree in the two earthquakes.

Repeated surveys using explosions at the Landers rupture zone have shown that the fault is healing (restrengthening) after the 1992 M 7.4 earthquake (Li *et al.*, 1998b; Li and Vidale, 2001). The fault-zone trapped waves recorded at the San Jacinto fault zone near Anza, California, also showed the existence of a soft wave guide on the Casa Loma fault strand that ruptured in the 1918 M 6.9 earthquake, but no clear wave guide for the strands (e.g., Hot Springs fault) that have not broken in the recent prehistoric times (Li *et al.*, 1997). These observations support a broken-then-healing cycle on active faults.

In Figure 9, we summarize our observations of velocity increases measured from waveform cross-correlations of the recordings for the same shot-receiver pairs between 2000 and 2001. The results show that shear velocities of fault-zone rocks that were damaged in the 1999 Hector Mine earthquake increased by $\sim 0.5\%$ – 1.0% between 2000 and 2001, with a smaller velocity increase of $\sim 0.3\%$ for surrounding rocks. This trend indicates that the Hector Mine rupture zone rigidity increased after the mainshock, most likely due to the closure of cracks that opened during the 1999 earthquake.

This process may be interpreted as reductive dilatancy (Nur, 1972). Estimates of the change in velocity due to the change in the density of cracks may be calculated using equations in which the elastic constants of fractured rock are functions of the crack density (O'Connell and Budiansky, 1974). We assumed randomly oriented cracks and computed the change in apparent crack density from measured changes in seismic velocity. The apparent crack density is defined by $\varepsilon = N(a^3)/V$, where a is the radius of the flat penny-shaped crack and N is the number of cracks in a volume V . We assumed cracks to be partially water filled, inferred by our measured $\Delta t_p/\Delta t_s$ of 0.725, and estimated that Poisson's ratio is 0.33. For the calculation, we used an average $V_p = 2.0$ km/sec and $V_s = 1.0$ km/sec for the fault-zone rock at shallow depth. These values are consistent with the velocity structure model for the shallow Hector Mine rupture zone (Li *et al.*, 2002). Our calculations revealed that the apparent crack density within the rupture zone decreased by 0.015 between 2000 and 2001, which caused $\sim 2\%$ increase in shear rigidity of the fault-zone rock.

We have considered the possibility of aligned cracks, but closure of isotropically oriented cracks is more consistent with the observed $\Delta t_p/\Delta t_s$. For fault-parallel aligned

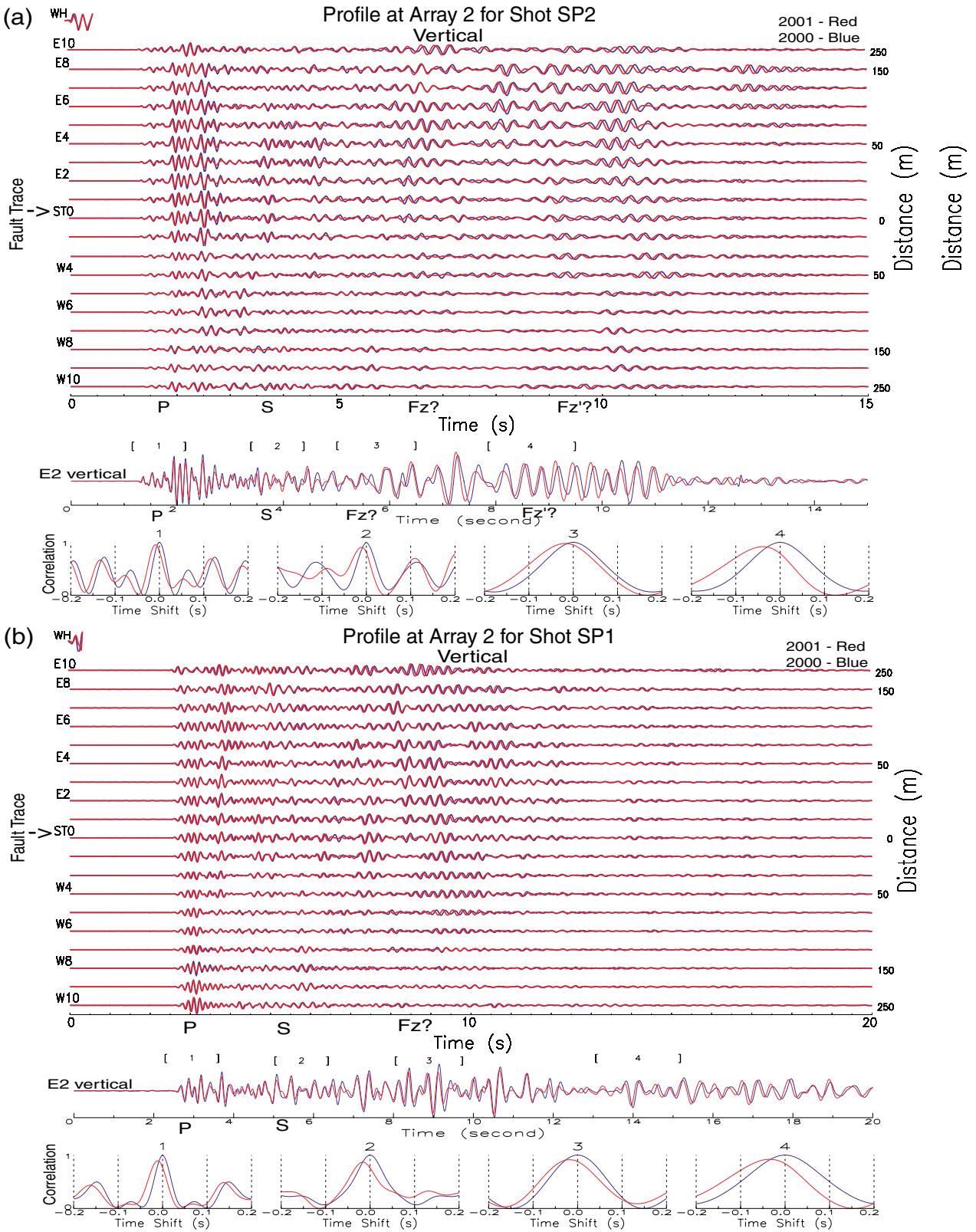


Figure 7. (a) Top: Vertical-component seismograms recorded at southeast array 2 for the north shot SP2 in 2000 and 2001. Seismograms have been bandpass (2–8 Hz) filtered and are plotted using a common scale for all traces. *P* and *S* waves arrive at ~1.8 and ~3.5 sec. Similar waveforms were recorded, but waves traveled faster in 2001 than in 2000. The wave trains like fault-zone trapped waves appear between 5 and 12 sec at stations on the east side of array 2. “WH” denotes the station located at the wellhead of SP2. Autocorrelations (blue lines) of seismograms in 2000 and cross-correlations (red lines) of recordings at station E2 in 2000 and 2001 are shown for four time windows (1–4 respectively). Seismograms have been bandpass (3–10 Hz) filtered. Other notations are the same as in Figure 3. (b) Same as in (a), but for the south shot SP1.

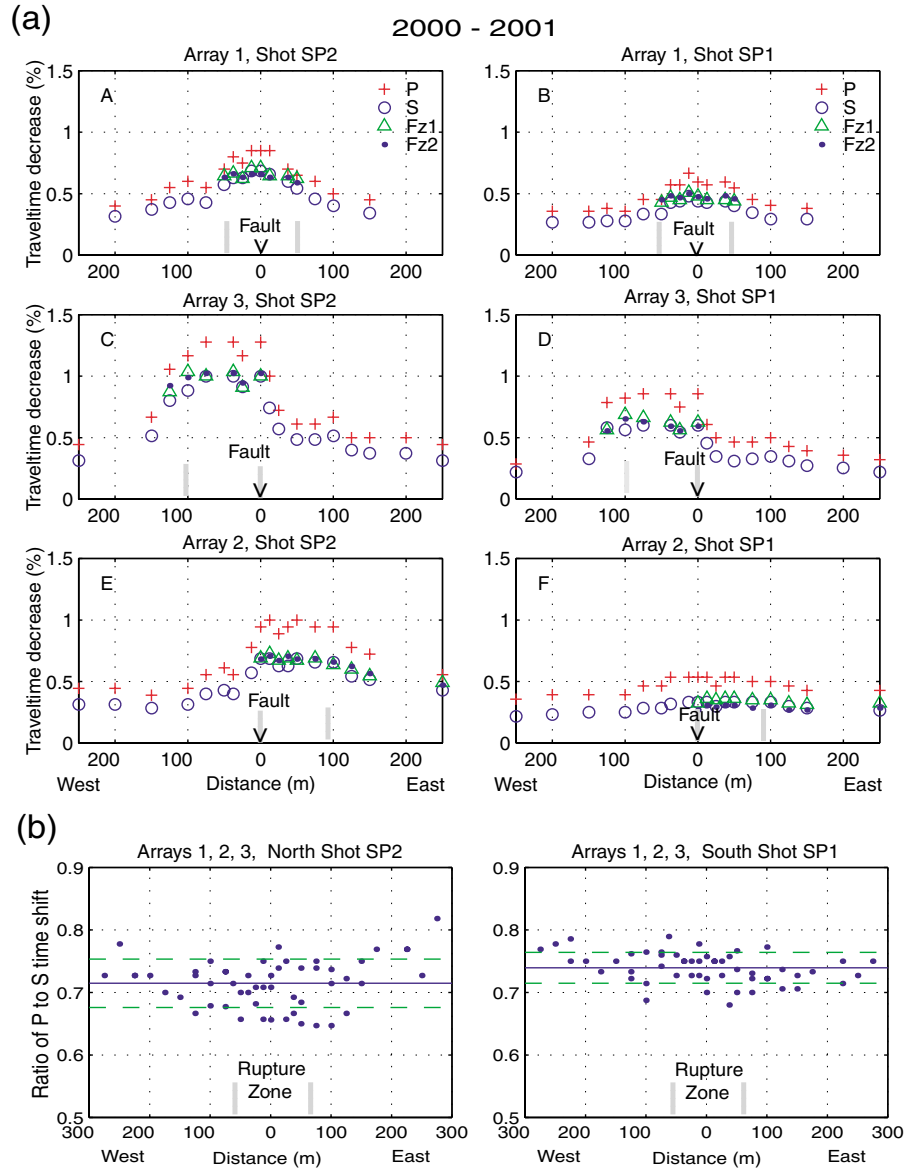


Figure 8. (a) Travel-time decreases in percentage for P , S , and fault-zone trapped waves determined from cross-correlations of seismograms recorded at arrays 1, 2, and 3 for shots SP1 and SP2 detonated within the Hector Mine rupture zone in October 2000 and November 2001. Six shot-array pairs are labeled A–F. The fault trace (marked by a black arrow) is at the center of the array in each frame. A pair of vertical gray bars in each frame denotes the zone with larger travel-time changes. The largest change in travel time was registered at array 3 across the middle LLF for the north shot SP2, while the smallest change was registered at array 2 across the southeast BF for the south shot SP1. (b) Ratio of travel-time decrease between 2000 and 2001 for P and S waves at three arrays (left) for the north shot SP2 and (right) for the south shot SP1. We have aligned the station with maximum travel-time change in each array at the center of the frame (distance of 0 m). The mean ratio is denoted by a solid line, and the standard deviation is denoted by dashed lines.

cracks, either wet or dry, Δt_p is much smaller than Δt_s ($\Delta t_p \sim 0.33\Delta t_s$), so closure of aligned cracks does not affect P waves nearly as much as it affects S waves. In reality, the cracks are probably not isotropically oriented and there may be some alignment according to the stress regime. However, the coherence is not simple to predict due to the stress var-

iations along the fault and may also change with time, as observed at the Nojima fault in Japan (Todokoro *et al.*, 1999). According to equations for the elastic moduli of the medium with isotropically oriented penny-shaped cracks (Garbin and Knopoff, 1975), we obtain

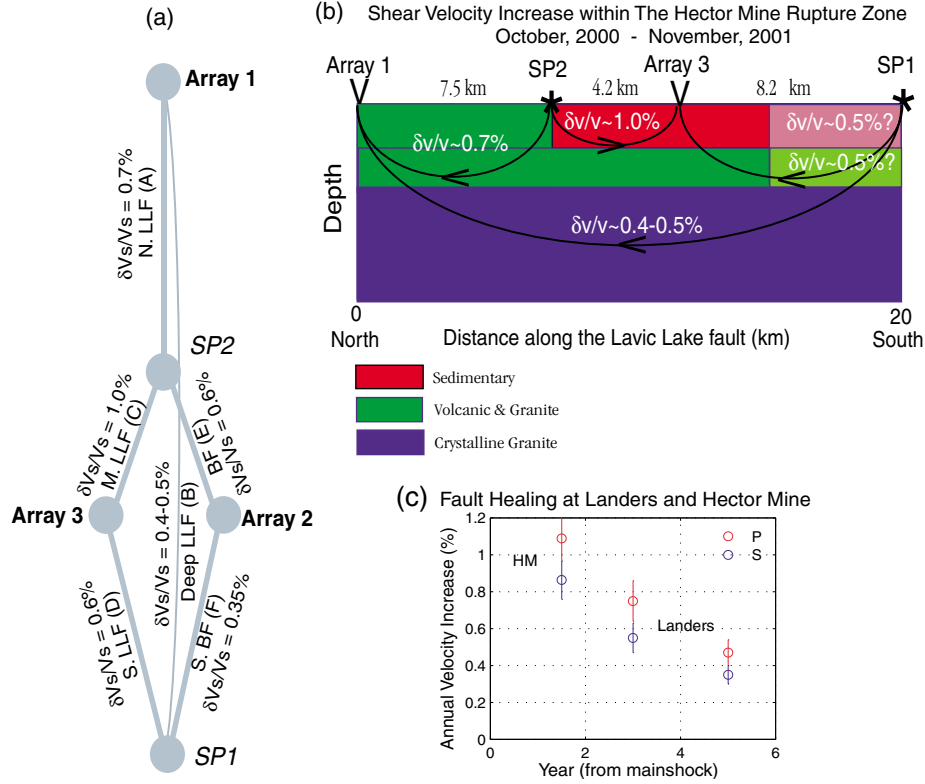


Figure 9. (a) Shear-velocity increases within the Hector Mine rupture zone between 2000 and 2001 determined from measurements of travel-time decreases for each shot-array pair of arrays 1–3 and shots SP1 and SP2. The value of velocity increase for each shot-array pair is the average of measurements at stations located within the rupture zone. The velocity increase varies between segments (labeled A–F), with the greatest change on the middle LLF and the smallest change on the southern BF. (b) The depth section shows shear velocity increases along the LLF between north array 1 and south shot SP1 during 2000–2001, with the greater changes at the shallow depth. However, the velocity increase was smaller in the southernmost part of LLF, where the rupture diminished. The standard deviations of velocity measurements are around 0.1%. (c) Percentage velocity increase per year on the Landers southern rupture zone and Hector Mine middle rupture zone after the 1992 Landers and 1999 Hector Mine earthquakes, respectively. Year 0 denotes the occurrence of the mainshocks. Color circles are the mean values for P and S waves with error bars. “HM” denotes the measurements at the Hector Mine rupture zone between 2000 and 2001, while “Landers” denotes the measurements at the Landers rupture zone between 1994 and 1996 and between 1996 and 1998.

$$\frac{1}{V_p} = \left\{ \frac{\rho}{3\mu} [1 + 2.49\varepsilon] \right\}^{1/2}, \quad \frac{1}{V_s} = \left\{ \frac{\rho}{\mu} [1 + 1.18\varepsilon] \right\}^{1/2}$$

for a Poisson solid, in which $\lambda = \mu$, with dry cracks, and

$$\frac{1}{V_p} = \left\{ \frac{\rho}{3\mu} [1 + 0.406\varepsilon] \right\}^{1/2}, \quad \frac{1}{V_s} = \left\{ \frac{\rho}{\mu} [1 + 0.914\varepsilon] \right\}^{1/2}$$

with water-saturated cracks, where V_p and V_s are velocities of P and S waves, ε is crack density, ρ is rock density, and λ and μ are bulk and shear modulus. Thus, the ratio of travel-time changes for P and S waves in a Poisson solid is

$$\frac{\Delta t_p}{\Delta t_s} = \left(\frac{2.490}{1.180} \right) \left(\frac{\mu}{\lambda + 2\mu} \right)^{1/2} = 1.22$$

for dry cracks and

$$\frac{\Delta t_p}{\Delta t_s} = \left(\frac{0.406}{0.914} \right) \left(\frac{\mu}{\lambda + 2\mu} \right)^{1/2} = 0.27$$

for water-saturated cracks. More precisely, in our study area, the rock has an anomalous Poisson’s ratio such that the P-wave velocity is about twice the S-wave velocity. In this case, $\Delta t_p/\Delta t_s$ is predicted to be 1.64 for dry cracks and 0.17 for wet cracks. So, the mean value of the $\Delta t_p/\Delta t_s$ ratio (~ 0.72) observed at the Hector Mine rupture zone would indicate that cracks within and near the rupture zone were partially water filled after the 1999 earthquake. We also note that this ratio was $\sim 10\%$ smaller within the rupture zone on the middle LLF at the shallow depth, suggesting that fault-

zone rock would be characterized by higher fluid saturation than surrounding rocks.

As shown in Figure 9a,b, the healing rate varied from one fault segment to another and with depth. This variation suggests that a fault may regain strength at a different rate that depends upon depth-dependent heterogeneity of rock type and slip and stress distributions, as well as rheology along the rupture zone. We tentatively interpret that the rupture zone on the middle LLF at shallow depth in a region with larger slip and soft sedimentary rock would inflict greater damage due to elastic response and strong shaking, and thus greater healing occurred. Dynamic rupture models may also help to delineate the connection between fault slip and the width and severity of the damage zone.

Figure 9c shows the annual healing rate with velocity increases on the Hector Mine rupture zone between 1 and 2 years after the 1999 mainshock and for larger intervals on the Landers rupture zone after the 1992 mainshock at a similar shallow depth. The velocity increases are taken from average travel-time decreases at stations of array 1 and array 3 located within the Hector Mine rupture zone for the north shot SP2 (Fig. 8a) and at stations within the Landers rupture zone (Fig. 4; Li and Vidale, 2001), respectively. At Hector Mine, the velocities increased by $\sim 1.1\%$ for P waves and $\sim 0.85\%$ for S waves on average for the middle and north LLF between 1 and 2 years after the 1999 mainshock. At Landers, the velocities increased by $\sim 0.77\%$ for P waves and $\sim 0.58\%$ for S waves on the Johnson Valley fault per year between 2 and 4 years after the 1992 mainshock and further increased by $\sim 0.47\%$ for P waves and 0.35% for S waves per year between 4 and 6 years after the mainshock. The Landers observations show that the healing rate decreased with time. It suggests that a fault may regain strength rapidly in the early stage of the interseismic period, but may take a long time to fully recover the strength for the next earthquake on it. We will continue to monitor the Hector Mine rupture zone to see if its healing rate slows, as did the healing rate at Landers.

During the fault healing, the reduction of crack density may be controlled by a combination of mechanical and chemical processes on the active fault. Fault healing may be affected by time-dependent frictional strengthening (Vidale *et al.*, 1994; Marone *et al.*, 1995; Marone, 1998; Schaff *et al.*, 1998), fluid variations or changes in the state of stress (Palmer *et al.*, 1995; Dodge and Beroza, 1997; Blanpied *et al.*, 1998), cementation, recrystallization, pressure solution, crack sealing, and grain contact welding (Hickman and Evans, 1992; Sleep and Blanpied, 1992; Olsen *et al.*, 1998), as well as the fault-normal compaction of the rupture zone (Massonnet *et al.*, 1996). Little chemical healing is expected from mineralogical lithification of gouge materials like quartz arenites at depths less than 3 km, although the interseismic healing due to chemical process may have a significant effect over longer time periods at seismogenic depth (Angevine *et al.*, 1982; Angevine and Turcotte, 1983). However, the "crack dilatancy" mechanisms associated with the

earthquake we discussed previously are likely to operate for fault healing with the time observed at shallow depth in our experiments using near-surface explosions, even if other processes are active too. Baisch and Bokelmann (2001) have found scattering change and temporal recovery near the Loma Prieta source region in the 5 years after the mainshock. They suggest that coseismic deformation might lead to crack opening either by local concentrations of shear stress or by elevated pore fluid pressure. After the earthquake, relaxational processes, such as crack healing, fluid diffusion, and postseismic deformations caused the cracks to close again with a logarithmic recovery rate.

Our observed ratio of P to S travel-time decrease (0.725) is lower than the predicted ratio (1.22) for dry cracks, so some fluid is probably present in cracks after an earthquake. We have found that the cracks became more wet with time at the Landers rupture zone (Li and Vidale, 2001). This may be due to the feedback of fluids into the fault zone in the interseismic period or due to the closure of cracks. At the Nojima fault of the 1995 M 7.1 Kobe earthquake, high porosity was measured (Ito, 1996), and high permeability and low strength were also measured in a damage zone to be about 40 m wide and centered at the main fault trace at shallow depth (Lockner *et al.*, 2000). This zone acted as a fluid conduit, and its width is consistent with the width of low-velocity wave guide on the Nojima fault delineated from fault-zone trapped waves (e.g., Ito and Kuwahara, 1995; Li *et al.* 1998a). The higher permeability within the damage zone (low-velocity wave guide) may correspond to a higher porosity than in the surrounding rocks, even though every crack includes a similar fraction of fluids. The reduction in apparent crack density within the rupture zone might be detectable in repeated measurements of porosity and permeability.

Signs of reduction in apparent crack density may have been detected in geodetic measurements. As rocks heal, there can be either more of the right-lateral shear deformation from the regional stress field that dominates the coseismic displacements or fault-normal compression from the reduction in volume. For the 1989 Loma Prieta, California, earthquake, there is evidence of several centimeters per year of fault-normal contraction in the years following the event (Burgmann *et al.*, 1997). Fault-normal contraction (~ 20 – 30 mm at surface) for the Landers rupture zone with a timescale of several years has also been reported (Massonnet *et al.*, 1996). At Landers, synthetic aperture radar images revealed uplift and depression with a 1 year timescale that is consistent with re-equilibration of pore fluids due to mainshock-induced stresses (Peltzer *et al.*, 1998).

In our study, we conclude that some cracks that had opened during the mainshock closed soon thereafter. This is consistent with our tentative interpretation of the soft low-velocity fault-zone wave guides on the Hector Mine and Landers rupture zones as being at least partially created during the mainshock, but with a possibly significant cumulative aspect as well. The broken-then-healing process on ac-

tive faults could be associated with substantial, inelastic, permanent deformation which creates the lower velocity and lower Q fault zone over time.

The results from fault-zone trapped waves recorded at Landers and Hector Mine rupture zones also help us understand the extent of damage to the rock mass in the fault zone and estimate dynamic stresses and nonlinear energy dissipation in fault zones during rupture by numerical modeling. Coupled with models of the coseismic rupture and slip processes, we are gradually obtaining a clearer picture of the physical and chemical processes taking place on faults during the earthquake cycle.

Acknowledgments

This study was supported by NSF Grant EAR-0001132 and partly by the Southern California Earthquake Center. SCEC is funded by NSF Cooperative Agreement EAR-8920136 and USGS Cooperative Agreements 14-08-0001-A0899 and 1434HQ97AG01718. Special acknowledgments to the Marine Corps Air Ground Combat Center (MCAGCC). Twenty-nine Palms, California, for their permission to carry out the experiment in the base and their invaluable help when we deployed instruments in the Bullion Mountains. We thank L. Jones of the USGS for her coordination of our initial recording of trapped waves at the Hector Mine rupture zone and Karl Gross of the USGS for his coordination of our experiments in the marine base. Tom Burdette of the USGS detonated explosions. We thank Sarah Gonzalez, Chris Lynch, Rob Mellors, Yihong Wang, and Fei Xu for their work in the field experiment. We appreciate the support of IRIS-PASSCAL Instrument Center for the use of their instruments and thank Mark Alvarez and Mike Fort for their collaboration in the experiment, as well as P. Davis for the use of UCLA battery chargers. We thank associate editor Gotz Bokelmann and reviewers David Schaff and Stefan Baisch for their helpful suggestions and comments on the manuscript. We also thank H. Houston, P. Shearer, M. Simons, and F. Vernon for valuable discussions in this study. The SCEC contribution number for this paper is 685.

References

- Aki, K. (1984). Asperities, barriers, characteristic earthquakes, and strong motion prediction, *J. Geophys. Res.* **89**, 5867–5872.
- Angevine, C. L., and D. L. Turcotte (1983). Porosity reduction by pressure solution: a theoretical model for quartz arenites, *Geol. Soc. Am. Bull.* **94**, 1129–1134.
- Angevine, C. L., D. L. Turcotte, and M. D. Furnish (1982). Pressure solution lithification as a mechanism for the stick-slip behavior of faults, *Tectonics* **1**, 151–160.
- Baisch, S., and G. H. R. Bokelman (2001). Seismic waveform attributes before and after the Loma Prieta earthquake: scattering change near the earthquake and temporal recovery, *J. Geophys. Res.* **106**, 16,323–16,337.
- Beroza, G. C., A. T. Cole, and W. L. Ellsworth (1995). Stability of coda wave attenuation during the Loma Prieta, California, earthquake sequence, *J. Geophys. Res.* **100**, 3977–3987.
- Blanpied, M. L., D. A. Lockner, and J. D. Byerlee (1992). An earthquake mechanism based on rapid sealing of faults, *Nature* **359**, 574–576.
- Blanpied, M. L., C. J. Marone, D. A. Lockner, J. D. Byerlee, and D. P. King (1998). Quantitative measure of the variation in fault rheology due to fluid-rock interactions, *J. Geophys. Res.* **103**, 9691–9712.
- Burgmann, R., P. Segall, M. Lisowski, and J. Svarc (1997). Post-seismic strain following the 1989 Loma Prieta earthquake from GPS and leveling measurements, *J. Geophys. Res.* **102**, 4933–4955.
- Byerlee, J. (1990). Friction, overpressure and fault-normal compression, *Geophys. Res. Lett.* **17**, 2109–2112.
- Chester, F. M., J. P. Evans, and R. L. Biegel (1993). Internal structure and weakening mechanisms of the San Andreas fault, *J. Geophys. Res.* **98**, 771–786.
- Cowie, P. A., and C. H. Scholz (1992). Growth of faults by accumulation of seismic slip, *J. Geophys. Res.* **97**, 11,085–11,095.
- Das, S., and K. Aki (1977). Fault plane with barriers: a versatile earthquake model, *J. Geophys. Res.* **82**, 5658–5670.
- Dieterich, J. H. (1972). Time-dependent friction in rocks, *J. Geophys. Res.* **77**, 3690–3697.
- Dieterich, J. H. (1978). Time-dependent friction and the mechanics of strike-slip, *Pure Appl. Geophys.* **116**, 790–806.
- Dodge, D., and G. C. Beroza (1997). Source array analysis of coda waves near the 1989 Loma Prieta, California mainshock: implications for the mechanism of coseismic velocity changes, *J. Geophys. Res.* **102**, 24,437–24,458.
- Garbin, H. D., and L. Knopoff (1975). Elastic moduli of a medium with liquid-filled cracks, *Q. Appl. Math.* **32** (October), 301–303.
- Harris, R. A., and S. M. Day (1997). Effects of a low-velocity zone on a dynamic rupture, *Bull. Seismol. Soc. Am.* **87**, 1267–1280.
- Hickman, S. H., and B. Evans (1992). Growth of grain contacts in halite by solution-transfer: implications for diagenesis, lithification, and strength recovery, in *Fault Mechanics and Transport Properties of Rocks*, B. Evens and T.-F. Wong (Editors), Academic, New York, 253–280.
- Ito, H. (1996). Structure and physical properties of the Nojima fault, Presented at U.S.-Japan Natural Resources 10th Biennial Meeting, Pasadena, California, 12–14 November 1996.
- Ito, H., and Y. Kuwahara (1995). Trapped waves along the Nojima fault from the aftershock of Kobe earthquake, 1995 (abstract), *EOS* **76** (Fall Meet. Supp.), F377.
- Ji, C., D. J. Wald, and D. V. Helmberger (2002). Source description of the 1999 Hector Mine, California earthquake. II. Complexity of slip history, *Bull. Seism. Soc. Am.* **92**, 1208–1226.
- Kanamori, H. (1994). Mechanics of earthquakes, *Ann. Rev. Earth Planet. Sci.* **22**, 207–237.
- Li, Y. G., and J. E. Vidale (1996). Low-velocity fault-zone guided waves: numerical investigations of trapping efficiency, *Bull. Seismol. Soc. Am.* **86**, 371–378.
- Li, Y. G., and J. E. Vidale (2001). Healing of the shallow fault zone from 1994–1998 after the 1992 $M7.5$ Landers, California, earthquake, *Geophys. Res. Lett.* **28**, 2999–3002.
- Li, Y. G., K. Aki, D. Adams, A. Hasemi, and W. H. K. Lee (1994a). Seismic guided waves trapped in the fault zone of the Landers, California, earthquake of 1992, *J. Geophys. Res.* **99**, 11,705–11,722.
- Li, Y. G., K. Aki, J. E. Vidale, and M. G. Alvarez (1998a). A delineation of the Nojima fault ruptured in the $M7.2$ Kobe, Japan, earthquake of 1995 using fault-zone trapped waves, *J. Geophys. Res.* **103**, 7247–7263.
- Li, Y. G., K. Aki, J. E. Vidale, and F. Xu (1999). Shallow structure of the Landers fault zone from explosion-generated trapped waves, *J. Geophys. Res.* **104**, 20,257–20,275.
- Li, Y. G., F. L. Vernon, and K. Aki (1997). San Jacinto fault-zone guided waves: a discrimination for recently active fault strands near Anza, California, *J. Geophys. Res.* **102**, 11,689–11,701.
- Li, Y. G., J. E. Vidale, K. Aki, C. J. Marone, and W. H. K. Lee (1994b). Fine structure of the Landers fault zone: segmentation and the rupture process, *Science* **256**, 367–370.
- Li, Y. G., J. E. Vidale, K. Aki, and F. Xu (2000). Depth-dependent structure of the Landers fault zone from trapped waves generated by aftershocks, *J. Geophys. Res.* **105**, 6237–6254.
- Li, Y. G., J. E. Vidale, K. Aki, F. Xu, and T. Burdette (1998b). Evidence of shallow fault zone strengthening after the 1992 $M7.5$ Landers, California, earthquake, *Science* **279**, 217–219.
- Li, Y. G., J. E. Vidale, S. M. Day, and D. Oglesby (2002). Study of the $M7.1$ Hector Mine, California, earthquake fault plan by fault-zone trapped waves, Hector Mine Earthquake Special Issue. *Bull. Seism. Soc. Am.* **92**, 1318–1332.

- Li, Y. G., J. E. Vidale, D. Oglesby, S. M. Day, and E. Cochran (2003). Multiple-fault rupture of the M7.1 Hector Mine, California, earthquake from fault-zone trapped waves, *J. Geophys. Res.* (in press).
- Lockner, D. A., H. Naka, H. Tanaka, H. Ito, and R. Ikeda (2000). Permeability and strength of core samples from the Nojima fault of the 1995 Kobe earthquake, in Proc. of the International Workshop on the Nojima Fault Core and Borehole Data Analysis, H. Ito, K. Fujimoto, H. Tanaka, and D. A. Lockner (Editors), Tsukuba, Japan, 22–23 November, 1999. *U.S. Geol. Surv. Open-File Rep. 00-129*, 147–152.
- Marone, C. (1998). The effect of loading rate on static friction and the rate of fault healing during the earthquake cycle, *Nature* **391**, 69–72.
- Marone, C., J. E. Vidale, and W. L. Ellsworth (1995). Fault healing inferred from time dependent variations in source properties of repeating earthquakes, *Geophys. Res. Lett.* **22**, 3095–3098.
- Massonnet, D., W. Thatcher, and H. Vadon (1996). Detection of postseismic fault-zone collapse following the Landers earthquake, *Nature* **382**, 612–616.
- Mooney, W. D., and A. Ginzburg (1986). Seismic measurements of the internal properties of fault zones, *Pure Appl. Geophys.* **124**, 141–157.
- Nur, A., (1972). Dilatancy, pore fluid, and premonitory variations of *ts/tp* travel times, *Bull. Seism. Soc. Am.* **62**, 1217–1222.
- O'Connell, R. J., and B. Budiansky (1974). Seismic velocities in dry and saturated cracked solids, *J. Geophys. Res.* **79**, 5412–5426.
- Olsen, M., C. H. Scholz, and A. Leger (1998). Healing and sealing of a simulated fault gouge under hydrothermal conditions for fault healing, *J. Geophys. Res.* **103**, 7421–7430.
- Palmer, R., R. Weldon, E. Humphreys, and F. Saucier (1995). Earthquake recurrence on the southern San Andreas modulated by fault-normal stress, *Geophys. Res. Lett.* **22**, 535–538.
- Papageorgiou, A. S., and K. Aki (1983). A specific barrier model for the quantitative description of inhomogeneous faulting and the prediction of strong motion. I. Description of the model, *Bull. Seismol. Soc. Am.* **73**, 693–722.
- Peltzer, G., P. Rosen, F. Rogez, and K. Hudnut (1998). Poroelastic rebound along the Landers 1992 earthquake surface rupture, *J. Geophys. Res.* **103**, 30,131–30,145.
- Rice, J. R. (1980). The mechanics of earthquake rupture, in *Physics of the Earth's Interior*, A. M. Dziewonski and E. Boschi (Editors), North-Holland, Amsterdam, 555–649.
- Rice, J. R. (1992). Fault stress states, pore pressure distributions, and the weakness of the San Andreas fault, in *Fault Mechanics and Transport Properties of Rocks*, B. Evans and T.-F. Wong (Editors), Academic, New York, 475–503.
- Sauber, J., W. Thatcher, S. C. Solomon, and M. Lisowski (1994). Geodetic slip rate for the eastern California shear zone and the recurrence time of Mojave Desert earthquakes, *Nature* **367**, 264–266.
- Scientists from the USGS, SCEC, and CDMG (2000). Preliminary report on the 16 October 1999 M7.1 Hector Mine, California, earthquake, *Seism. Res. Lett.* **71**, 11–23.
- Schaff, D., G. C. Beroza, and B. E. Shaw (1998). Postseismic response of repeating aftershocks, *Geophys. Res. Lett.* **25**, 4549–4552.
- Scholz, C. H. (1990). *The Mechanics of Earthquakes and Faulting*, Cambridge U Press, New York.
- Sibson, R. H. (1977). Fault rocks and fault mechanisms, *J. Geol. Soc. London* **133**, 191–213.
- Sibson, R. H. (1982). Fault zone models, heat flow, and the depth distribution of earthquakes in the continental crust of the United States, *Bull. Seismol. Soc. Am.* **72**, 151–163.
- Sieh, K., L. Jones, E. Hauksson, K. Hudnut, D. Eberhart-Phillips, T. Heaton, S. Hough, K. Hutton, H. Kanamori, A. Lilji, S. Lindvall, S. McGill, J. Mori, C. Rubin, J. Spotila, J. Stock, H. Thio, J. Treiman, B. Wernick, and J. Zachariasen (1993). Near-field investigations of the Landers earthquake sequence, April to July 1992, *Science* **260**, 171–176.
- Sleep, N. H., and M. L. Blanpied (1992). Creep, compaction, and the weak rheology of major faults, *Nature* **359**, 687–692.
- Tadokoro, K., M. Ando, and Y. Umeda (1999). S wave splitting in the aftershock region of the 1995 Hyogo-ken Nanbu earthquake, *J. Geophys. Res.* **104**, 981–991.
- Vidale, J. E., W. L. Ellsworth, A. Cole, and C. Marone (1994). Rupture variation with recurrence interval in eighteen cycles of a small earthquake, *Nature* **368**, 624–626.
- Walder, J., and A. Nur (1984). Porosity reduction and crustal pore pressure development, *J. Geophys. Res.* **89**, 11,539–11,548.
- Wesson, R. L., and W. L. Ellsworth (1973). Seismicity preceding moderate earthquakes in California, *J. Geophys. Res.* **78**, 8527–8545.

Department of Earth Sciences
University of Southern California
Los Angeles, California 90089-0740
ygli@terra.usc.edu
(Y.G.L.)

Department of Earth and Space Sciences
University of California
Los Angeles, California 90095
vidale@moho.ess.ucla.edu
(J.E.V., E.C.)

Department of Geological Sciences
San Diego State University
San Diego, California 92182
day@moho.sdsu.edu
(S.M.D.)

Department of Earth Sciences
University of California
Riverside, California 92521
doglesby@namazu.ucr.edu
(D.D.O.)